Journal of Experimental Botany
https://doi.org/10.1093/jxb/erab538 Advance Access Publication 19 January, 2022

RESEARCH PAPER

Chemical genetics in *Silene latifolia* elucidate regulatory pathways involved in gynoecium development

Václav Bačovský[1,*], Radim Čegan[1,*], Eva Tihlaříková[2], Vilém Neděla[2], Vojtěch Hudzieczek[1], Lubomír Smrža[1], Tomáš Janíček[1], Vladimír Beneš[3] and Roman Hobza[1,†]

[1] Department of Plant Developmental Genetics, Institute of Biophysics of the Czech Academy of Sciences, Kralovopolska 135, 612 65 Brno, Czech Republic
[2] Environmental Electron Microscopy Group, Institute of Scientific Instruments of the Czech Academy of Sciences, Kralovopolska 147, 612 64 Brno, Czech Republic
[3] EMBL Genomics Core Facility, EMBL Heidelberg, Meyerhofstraße 1, D-69117 Heidelberg, Germany

* These authors contributed equally to this work.
† Correspondence: hobza@ibp.cz

Received 9 July 2021; Editorial decision 2 December 2021; Accepted 9 December 2021

Editor: Madelaine Bartlett, University of Massachusetts Amherst, USA

Abstract

Dioecious plants possess diverse sex determination systems and unique mechanisms of reproductive organ development; however, little is known about how sex-linked genes shape the expression of regulatory cascades that lead to developmental differences between sexes. In *Silene latifolia*, a dioecious plant with stable dimorphism in floral traits, early experiments suggested that female-regulator genes act on the factors that determine the boundaries of the flower whorls. To identify these regulators, we sequenced the transcriptome of male flowers with fully developed gynoecia, induced by rapid demethylation in the parental generation. Eight candidates were found to have a positive role in gynoecium promotion, floral organ size, and whorl boundary, and affect the expression of class B MADS-box flower genes. To complement our transcriptome analysis, we closely examined the floral organs in their native state using field emission environmental scanning electron microscopy, and examined the differences between females and androhermaphrodites in their placenta and ovule organization. Our results reveal the regulatory pathways potentially involved in sex-specific flower development in the classical model of dioecy, *S. latifolia*. These pathways include previously hypothesized and unknown female-regulator genes that act on the factors that determine the flower boundaries, and a negative regulator of anther development, *SUPERMAN-like* (*SlSUP*).

Keywords: Androhermaphrodite, dioecy, flower development, gynoecium, *HANABA TARANU* (*GATA18*), sex chromosomes, *Silene latifolia*, *SUPERMAN-like* (*SlSUP*).

Introduction

Sex determination in plant and animal species is driven by environmental cues (e.g. temperature affects the sex ratio in turtles) and by genetic factors located on the sex chromosomes (Abbott *et al.*, 2017). These factors control the development of female and male organs on different individuals and influence specific properties beyond sexual organogenesis, such as size,

weight, color, and behavioral functions (Hurst, 1996; Tanurdzic and Banks, 2004). The genetic basis of factors leading to separate male and female individuals in plants (dioecy) occurred many times independently, in diverse lineages, yet the molecular mechanisms remain mostly elusive (Renner, 2014; Charlesworth, 2016). In garden asparagus (*Asparagus officinalis*) (Harkess *et al.*, 2017) and kiwifruit (*Acitinidia chinensis*) (Akagi *et al.*, 2019), the existence of male activator and female suppressor genes supports the 'two-gene' sex determination model that posits two separate genes (usually in one linkage group, male and female sterility factors) in the evolution of dioecy (Cronk and Müller, 2020). An alternative mechanism was also described in poplar (*Populus trichocarpa*) and persimmon (*Diospyros kaki*) (Akagi *et al.*, 2014; Müller *et al.*, 2020), representing a single-gene-based mechanism. These two models imply that diverse upstream regulators control dioecy in plants. In turn, the upstream regulators may differ in the level of epigenetic histone marks and level of DNA methylation as shown for the anther regulator MeGI in Japanese persimmon (Akagi *et al.*, 2016), for the sex-determining region in *Populus balsamifera* (Bräutigam *et al.*, 2017), and selected X- and Y-linked alleles in *Silene latifolia* (Rodríguez Lorenzo et al., 2018, 2020; Bačovský *et al.*, 2019). Yet, in *S. latifolia*, a historical 'two-gene' sex determination model, the sex-determining region is still unknown since Westergaard characterized a gynoecium suppressor and stamen promotor region by using deletion mutants (Westergaard, 1946). This is, among other factors, mainly because of the locus complexity of the non-recombining region paired with the abundance of transposons (Hobza et al., 2015, 2018). Yet, it is recognized that the knowledge of upstream regulators will shed light on the origin of the sex-determining chromosome region in this plant in a complex view. This will also allow the study of the evolution of sex-determining genes in the background of XY, XYY, and ZW sex chromosome systems which originated from different pairs of autosomes (Renner and Müller, 2021).

In *S. latifolia*, early studies examined epigenetic regulation of gynoecium development in *S. latifolia* by treatment with 5-azacytidine (5-azaC), which is incorporated into DNA and inhibits DNA methyltransferases, causing DNA hypomethylation. The authors proposed three possible mechanisms for gynoecium development and suggested that epigenetically modified genomic regions undergo holandric inheritance (Janoušek et al., 1996, 1998). Several studies used biological treatment and smut fungus infection to cause an effect similar to that of 5-azaC treatment (Janoušek *et al.*, 1996), promoting female flower masculinization and male feminization (Kazama *et al.*, 2005; Zemp *et al.*, 2015; Kawamoto *et al.*, 2019). Although such experiments proved to be efficient for studying the developmentally important functions of flower-related genes, the atypical developmental changes were not heritable. Thus, the transcriptome expression profiles were not altered in the long term to reveal a complete set of candidate genes promoting flower organization (Kazama *et al.*, 2005; Hobza *et al.*, 2018). Several studies examined the role of MADS-box genes in flower development using *in situ* hybridization (Hobza *et al.*, 2018). Hardenack *et al.* (1994) suggested that gynoecium-suppressing or promoting genes may act on the factors that determine the boundaries of the whorls. Yet, none of such factors has been described to date, and the identity of sex determination as well as that of flower development genes remains elusive (reviewed in Hobza *et al.*, 2018; Renner and Müller, 2021).

Treatment with epigenetically active chemical agents (chemical genetics) alone and in combination is a common practice in transgenerational studies examining epigenetic regulation of various traits (Zhang *et al.*, 2013; Cruz and Becker, 2020). These traits are established through a new variety of differentially methylated regions (Bartels *et al.*, 2018; Zhang *et al.*, 2018), leading to allele expression repatterning and new phenotypic characteristics transmitted to the next generation (Reinders *et al.*, 2009; Baubec *et al.*, 2014; Pecinka and Liu, 2014). Such treatment is often used if mutants are not available or if specific interference with DNA in order to obtain new phenotypes is required (Pecinka and Liu, 2014). Like mutagenesis, chemical genetic approaches may result in pleiotropic effects and phenotypes that are not identical to genetic mutations (Baubec *et al.*, 2010; Pecinka and Liu, 2014), as shown for feminization of male flower buds in Japanese persimmon (Akagi *et al.*, 2016) and sex reversion in *S. latifolia* (Janoušek *et al.*, 1996). To examine the pleiotropic effects caused by chemical genetics, next-generation high-throughput RNA sequencing (RNA-seq) and transcriptome profiling are fundamental tools to understand the functional genomic elements in treated plants (Wang *et al.*, 2009; Shendure *et al.*, 2017). Transcriptome profiling already provided valuable information about the expression of important genes in many species and taxa (Mortazavi *et al.*, 2008; Wang *et al.*, 2009; Kumar and Trivedi, 2016; Shulse *et al.*, 2019), and has led to characterization of multiple regulatory pathways of important traits (Li *et al.*, 2009; Glazinska *et al.*, 2017; Quan *et al.*, 2019; Hu *et al.*, 2020; Howlader *et al.*, 2020; Kang *et al.*, 2020).

In this work, we aimed to address two important questions concerning flower development in *S. latifolia* using a combination of RNA-seq transcriptome profiling and precise phenotyping: First, what regulatory pathways are involved in gynoecium development in *S. latifolia*, and second, how are the principal regulatory pathways related to sex-specific gene expression and flower function? Using precise phenotyping with a field emission environmental scanning electron microscope (FE-ESEM), we describe how the atypical development of the gynoecium in males induced by chemical genetics affects androhermaphrodite fertility (individuals producing both male and bisexual flowers) and placenta organization. To identify the gene regulatory pathways involved in gynoecium development, we gathered the transcriptomes of males, females, and androhermaphrodites. and compared their expression profiles. Using this approach, we identified previously unknown

important regulatory sex-linked and autosomal genes. Based on Arabidopsis functional annotation for these candidates, eight genes were found to have a putative role in female (gynoecium) development and flower organization. We discuss the possible function of newly detected sex-linked genes in the context of previous results and propose a genetic model for gynoecium development. We show the expression of the upstream regulatory candidates and their hypothesized downstream targets, and the expression of the MADS-box gene in flower development in the well-established dioecious model, *S. latifolia*.

Materials and methods

Treatment data, drug concentration, and RNA extraction

Seedlings of *S. latifolia* inbred population U15 (seeds owned by Institute of Biophysics of the Czech Academy of Sciences), made by 15 generations of full-sib mating, were used as a parental population for all drug experiments. Efficient drug concentrations were estimated based on the literature (Lechner *et al.*, 1996; Baubec *et al.*, 2009) and an *in vitro* drug treatment assay (Supplementary Figs S1A–S3). Seeds were first sterilized and germinated (Bačovský *et al.*, 2019) and then grown on BMS-10 medium (Ye *et al.*, 1990) in a growth chamber with a 12 h photoperiod and 22 °C. Fresh BMS-10 supplemented by different concentrations of sodium butyrate (SB) (0.5, 1.0, 2.5, and 5.0 mM) and zebularine (ZEB) (10, 20, 30, and 40 μM) was replaced every 3 d for 2 weeks. As a control, the same concentrations of DMSO (for ZEB) or water (SB) were used. A 100 μl aliquot of 2.5 mM SB and 40 μM ZEB mixture (or in the case of the control, the same amount of DMSO and water) was injected into 4-week-old plants (F_0). Mixture injections were repeated every 3 d for 2 weeks after the first occurrence of flowering (Supplementary Fig. S1B). Plants were kept in a greenhouse under a 16 h light/8 h dark cycle at 24 °C in controlled conditions. Seeds derived from self-pollinated androhermaphrodite flowers and full-sib mating crosses in F_1 and F_2 were used to test the inheritance pattern of the androhermaphrodite phenotype. Three flowers of stage 11 within one individual for wild-type (WT) male, WT female, and F_1 (HF1) and F_2 androhermaphrodites (HF2) (two stigmas) were cut off the petals and sepals and were collected into liquid nitrogen.

RNA was isolated in biological triplicates based on Zluvova *et al.* (2010). To avoid the impact of the plant aging on RNA quality, only the first three flowers were collected. Total RNA was isolated according to the instructions of the manufacturer Norgen Biotek (Catalog no. 24400). DNA-free RNA was obtained following total RNA purification (Catalog no. 25710). The RNA purity was controlled using a ThermoFisher High-capacity RNA-to-cDNA kit (Catalog no. 4387406) and 36× cycles of PCR on an RNA and cDNA template using actin primers involving the intron sequence: Actin-F (5′-CAGGCCGTTCTCTCCTTGTA-3′) and Actin-R (5′-TCCACCACTGAGCACACAAT-3′).

Flower phenotyping

Flowers were opened with dissecting needles, and petals and sepals were carefully removed for final imaging and ovule and placenta examination. Final imaging and phenotyping of hermF0, hermF1, and hermF2 individuals and the type of placentation were examined under an Olympus microscope (SZX-ILLK200) supplemented by Optic illuminator W/dual bifurcated light guides (KL1500 LCD) and Olympus DF Plapo 1X-4. Each type of ovule and placenta and the number of ovules were determined in the first 10 individual flowers in WT females, androhermaphrodites, and females.

A pollen staining protocol (Peterson *et al.*, 2010) was followed with minor modifications. The anthers were first squeezed in the staining solution and later heated on a plate at 85 °C for 10 min, before final examination under an Olympus CX43microscope. Each experiment was repeated at least six times. The number of viable and non-viable pollen was counted in ImageJ FiJi (1.52p) using the Multi point Tool function. One-way ANOVA followed by Tukey's multiple comparisons test for pollen viability and ovule number was performed using GraphPad Prism version 8.0.0 for Windows (GraphPad Software, San Diego, CA, USA; www.graphpad.com). As a meaningful comparison, we compared males and females with androhermaphrodites. For morphological characterization of flowers in their fresh state free of any microstructural changes or artifacts, an FE-SEM (a field emission environmental scanning electron microscope) equipped for advanced control of thermodynamic conditions inside the specimen chamber (Neděla *et al.*, 2020), the wide field aperture detector (WFAD) for ESEM (newly developed for the purpose of this research at the ISI ASCR), and the ionization secondary electron detector with an electrostatic separator (ISEDS) were used (Neděla *et al.*, 2018). For FE-ESEM, sepals and petals were first cut off from stage 11 flowers in the same way as for phenotyping and RNA isolation. Electron micrographs of *S. latifolia* male, female, and androhermaphrodite flowers were obtained as reported in Neděla *et al.* (2015). The samples were placed in 2 μl of water on a flat cylindrical brass sample holder of the Peltier stage and processed according to a low temperature method for the FE-ESEM protocol (Neděla et al., 2015, 2016), without any artifacts caused by glutaraldehyde fixation, ethanol drying, or sputter-coating with platinum as previously reported. The observation conditions were water vapor pressure 150 Pa and sample temperature –20 °C. All experiments were performed using an FE-ESEM QUANTA 650FEG (Thermo Fisher Scinetific) with a beam accelerating voltage of 20 kV, a probe current of 30 pA, and a working distance of 13 mm. Micrographs were taken using a combination of the WFAD for wide field imaging in ESEM and the ISEDS for higher resolution imaging. Macrographic images of the whole flowers were made by composing micrographs using Maps software (Thermo Fisher Scientific).

RNA-seq library construction and sequencing

Transcriptome sequencing libraries were prepared from total RNA with the Illumina TruSeq mRNA Library Prep Kit at the Genomics Core Facility (Genecore, EMBL, Heidelberg). The sequencing of the libraries was conducted at the Genecore on Illumina NextSeq500 instrument with 75 bp paired-end reads.

RNA-seq data analysis

The quality of sequencing reads was inspected in FastQC (http://www.bioinformatics.babraham.ac.uk/projects/fastq). The *S. latifolia* U10 reference transcriptome (Zemp *et al.*, 2016) was verified by the Benchmarking Universal Single-Copy Ortholog (BUSCO) pipeline (Simão *et al.*, 2015). Read trimming on quality (Q30) and sequencing adaptor removal were done with Trimmomatic -0.32 (Bolger *et al.*, 2014). Cleaned reads from each library were pseudoaligned to the *S. latifolia* reference transcriptome (Muyle *et al.*, 2012), which originated from the U population, using Kallisto (version 0.45.0) (Bray *et al.*, 2016) with default parameters and with the number of bootstrap samples set to 100. The Kallisto index for reference fasta files was created with a k-mer length of 19. Transcript abundance estimations from Kallisto were used as input for differential expression analysis employing the Bioconductor DESeq2 package (version 1.24.0) (Love *et al.*, 2014). The generalized linear model approach was applied to all comparisons. Transcripts were considered as differentially

expressed when the adjusted *P*-value was <0.001 and log2 fold change was greater than ±1. Transcripts were annotated through comparisons with the Swissprot and UniprotKB complete proteome databases using the Trinotate pipeline (Supplementary Table S1) (Bryant *et al*., 2017). Gene Ontology (GO) enrichment among selected transcripts was done using Trinotate and the GOseq bioconductor package (Young *et al*., 2010). Clustering of differentially expressed genes (DEGs) was done by the bioconductor coseq package (Supplementary Appendix S1). All R scripts were run in R studio, and all software and tools used are listed in Supplementary Appendix S1). Transposable element (TE) expression was estimated using the SalmonTE pipeline (Jeong *et al*., 2018) and the *S. latifolia* TE reference library (Macas *et al*., 2011). First, using the SalmonTE index mode, we created the *S. latifolia* specific index file and quantified the TE expression values (in TPM; transcripts per million). Using the test mode, we performed the differential expression analysis for all comparisons.

Identification of sex-linked transcripts and expression analysis

Putative sex-linked transcripts were identified in the *S. latifolia* reference transcriptome (Zemp *et al*., 2016) by blast-n searches against previously published sets of sex-linked transcripts (Chibalina *et al*., 2011; Bergero *et al*., 2011; Muyle *et al*., 2012; Zemp *et al*., 2016; Papadopulos *et al*., 2015). For blast searches, blast-n with an e-value of 1E–40 from blast-all 2.2.26 was used (ftp://ftp.ncbi.nlm.nih.gov/blast/executables/). As sex-linked transcripts, we considered those with at least one hit against the above-mentioned datasets (Supplementary Table S2) Genes, potentially regulated by gynoecium-promoting candidates were selected from inferred pathways in the model plant Arabidopsis. The relative expression presents the log10 of average TMM (trimmed mean of M-values) Kallisto expression values.

Results

Epigenetic chemical treatment turns males into androhermaphrodites

Similarly to previous experiments (Janoušek et al., 1996, 1998), we induced hermaphrodite flower development in male individuals of *S. latifolia* (Fig. 1A) using two functionally diverse groups of chemical drugs (Nowicka *et al*., 2020): (i) zebularine (ZEB), a non-methylable cytidine analog; and (ii) sodium butyrate (SB), a histone deacetylase inhibitor. First, both drugs were screened for their optimal dose concentrations (Supplementary Fig. S1A). Second, the optimal dose concentrations were injected into adult *S. latifolia* plants before flowering, and, finally, the hermaphrodite flower trait was followed for two generations (Supplementary Figs S1B, S2, S3).

We examined the effect of optimal doses on adult plants for ZEB and SB separately and in combination (40 μM ZEB, 2.5 mM SB; Supplementary Fig. S3A–C). Due to little or no effect on plant growth in adult plants, we evaluated the treatment based on the phenotypic changes in male flower development: (i) plants with no effect; (ii) males turned into androhermaphrodites (individuals producing both male and bisexual flowers); and (iii) females (with or without prolongated stamens). As expected from the *in vitro* assay (Supplementary Appendix S1), ZEB and SB separately turned 20–30% of males in the population (n=128) into androhermaphrodites (Supplementary Fig. S3D). The combination of both drugs induced gynoecium development in almost 40% of males (Supplementary Fig. S3D). The control group of males and females in the *in vitro* assay contained no individuals with prolongated carpels or prolongated stamens. Next, we used flowers with both carpels (gynoecium) and stamens as pollen donors in the crossing experiment (Supplementary Fig. S2A). Again, almost 40% of the males in the F_1 population were androhermaphrodites (termed HF1), and all males in the F_2 population (termed HF2) were already androhermaphrodites (Supplementary Fig. S3E). As a control, we used non-treated (NT) males as pollen donors and pollinated treated females in the F_0 generation, or females in the androhermaphrodite progeny in F_1 and F_2 generations (directly after treatment or in the HF1 and HF2 generations). No androhermaphrodites resulted from such crosses (Supplementary Fig. S2B); hence, the hermaphrodite flower trait was transmitted only through the androhermaphrodite germline (Supplementary Fig. S2A). We observed four different types of androhermaphrodite individuals ($HF_{I–IV}$) and types of carpel (Fig. 1A). HF_I contained a strongly reduced ovary and atypically prolongated stigma. HF_{II} already consisted of one developed stigma as well as a suppressed stigma and an ovary without placenta. HF_{III} and HF_{IV} possessed 1–4 stigmas, but the size of the placenta was decreased compared with NT females (Fig. 1A). The inheritance of these flower traits was increased when more perfect flower types (functional ovary and stigmas) of androhermaphrodite type $HF_{III–IV}$ were used as pollen donors (Supplementary Fig. S3D, E). These results corroborate previous studies that the Y chromosome possesses a regulatory region (Westergaard, 1958; Kazama *et al*., 2016; Hobza *et al*., 2018) which is affected by epigenetic mechanisms in a heritable fashion, showing holandric inheritance and high androhermaphrodite flower trait penentrance in the second generation. Further, the higher percentage of androhermaphrodites from simulatenous treatment by both drugs (ZEB and SB) shows a non-redundant effect of both drugs.

Androhermaphrodite flowers contain defective carpels and fewer ovules

We studied detailed phenotypic changes caused by ZEB and SB using the combination of large-field and ISEDS morphology-sensitive detectors of secondary electrons (Neděla *et al*., 2018, 2020). We examined male and female flowers in the androhermaphrodite progeny using FE-ESEM and found differences at the cellular level in flower organization (Fig. 1B–K; Supplementary Fig. S4A–D). NT male flowers contained functional stamens and minor suppressed gynoecia (Fig. 1B, E, F). NT female flowers contained an ovary, five stigmas, and five suppressed anthers (Fig. 1C, G, H). The androhermaphrodite flower type HF_{III} possessed, apart from 10 stamens (two whorls), a fully fertile gynoecium

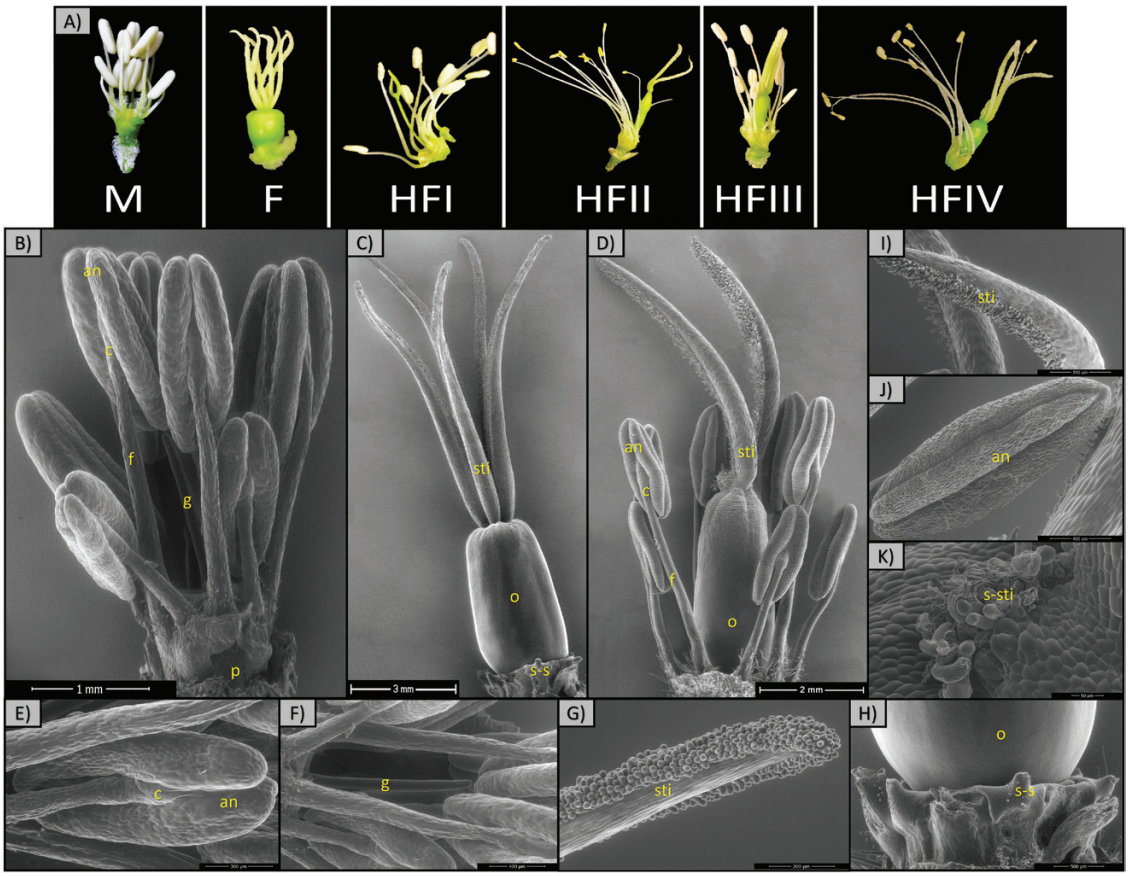

Fig. 1. Phenotyping of flower organs in *S. latifolia* male, female, and androhermaphrodite, and flower comparison using FE-ESEM. (A) Comparison of NT male, female, and four types of androhermaphrodite flowers. (B–D) FE-ESEM of a stage 11 NT male flower, an NT female flower, and an androhermaphrodite. (E and F) Detail of fully developed anther and rudimentary gynoecium in NT male flower. (G and H) Detail of fully developed stigma and suppressed stamen in NT female. (I–K) Detail of androhermaphrodite stigma, androhermaphrodite anther, and suppressed stigma. Note the differences in the carpel size and in the number of stigmas between NT females and androhermaphrodites (C, D). Anther (an), anther connective (c), filament (f), pedicel (p), gynoecium (g), stigma (sti), ovary (o), suppressed stigma (s-sti).

(Fig. 1D), consisting of an ovary, and stigmas having phenotypically functional anthers, and one suppressed stigma (Fig. 1D, I–K). Female carpels in the HF1 and HF2 generations were similar to NT females (Supplementary Fig. S4A–D). The flowers consisted of a functional ovary (Supplementary Fig. S4A–C), with 5–6 stigmas (Supplementary Fig. S4A, D) and, compared with NT females atypical suppressed stamens only (Supplementary Fig. S4C). Yet, androhermaphrodites possessed significantly higher numbers of aborted pollen compared with NT ($P<0.001$) (Supplementary Fig. S5A–I), reaching from 38% (wild type like, $HF_{III,IV}$) to almost 60% ($HF_{I,II}$) of non-viable pollen (Supplementary Fig. S5A–F). Thus, the androhermaphrodite individuals significantly differed from the control (>90% viable), $P<0.001$ (Supplementary Fig. S5I). In addition, the presence of aborted and viable pollen was confirmed by FE-ESEM (Supplementary Fig. S5G, H). All androhermaphrodites also significantly differed in the number of ovules ($P<0.001$) and, in some cases, the placental organization (HF_{IIIa} flowers had a marginal placenta, whereas more perfect androhermaphrodite flowers possessed a free central placenta similar to NT females) (Supplementary Fig. S6A–D). Thus, phenotypic changes in androhermaphrodites suggest that not only regulators setting correct development of carpel and stigma were affected but also genes which are responsible for organ size, ovule number, and placenta polarity (Figs 1D; Supplementary Fig. S6A, B).

Differential gene expression analysis in androhermaphrodites and RNA-seq data validation

To characterize the regulatory pathways related to carpel development in androhermaphrodites, we generated RNA-seq data for *S. latifolia* males, females, HF1, and HF2 (Fig. 1B–D). For 12 samples (triplicate samples for each variant), we obtained nearly 605 million paired-end raw sequencing reads (Supplementary Table S3). We observed that 1283 transcripts from 1440 had complete BUSCOs (Supplementary Table S4), and nearly 59% of the searched sequences were found in the Swissprot database. In the reference transcriptome, we

identified 2469 potentially sex-linked transcripts using the blast search algorithm (compared with available *S. latifolia* sex-linked gene datasets; Supplementary Table S2); 72–79% of the RNA-seq data were successfully pseudoaligned to the reference transcriptome (Supplementary Table S3). Genetic distance was examined by principal component analysis, and validated by Cook's distances and by sample-to-sample distances, differentiating all datasets to three clusters: males, females, and androhermaphrodites (and subclusters HF1 and HF2) (Supplementary Fig. S7A–C). Differential gene expression analysis in pairwise male:female (MvsF), male:androhermaphrodite F_1 (MvsHF1), male:androhermaphrodite F_2 (MvsHF2), female:androhermaphrodite F_1 (FvsHF1), female:androhermaphrodite F_2 (FvsHF2), and androhermaphrodite F_1:androhermaphrodite F_2 (HF1vsHF2) comparisons identified 15 325 DEGs. Among them, we examined 3782 DEGs in MvsF, 1809 in MvsHF1, 2621 in MvsHF2, 3119 in FvsHF1, 3465 in FvsHF2, and 529 in HF1vsHF2 (Supplementary Fig. S8A–F; Supplementary Table S5; Supplementary Dataset S1). From these comparisons, 4392 DEGs were used for identification of candidate genes involved in flower sex development in GO enrichment analysis and transcriptome profiling.

DNA- and histone methylation-related gene expression between sexes

We searched for candidates which show expression differences between sexes and are known for their function in transcriptional regulation in Arabidopsis (Supplementary Dataset S2). We performed expression profiling of genes related to histone modification (methylation, acetylation), DNA methylation, and DNA damage and stress response, as well as genes regulated directly by DNA methylation (epialleles). Using this profiling, we assessed differences in expression in androhermaphrodites compared with males and females (Fig. 2). Comparing the male, female, and androhermaphrodite flowers (MvsF, MvsHF1, MvsHF2, FvsHF1, FvsHF2, and H1vsHF2), we found that only several genes among selected regulators related to chromatin organization had distinct expression patterns between sexes (MvsF) and between floral phenotypes (MvsH1 and MvsH2). In these comparisons, the most distinct expression patterns were found for Arabidopsis homologs of *AGO4b* (Fig. 2A), *DDM1b*, *SUVH4b*, and *SUVR4* (Fig. 2B); *JMJ13* and *JMJ26* (Fig. 2C); *SOG1* (Fig. 2D); *HAC1c*, *HAF1*, *HDA8*, *HDA9*, *SRT1*, and *SRT2* (Fig. 2E); and *ABI3* and *ERECTA* (Fig. 2F). The differences in expression between sexes were also found in DNA damage response and stress-related genes down-regulated in females and hermaphrodites, namely for *ATMa*, *ATMb*, *ATRa*, *ATRb*, *ATRc*, *BRCA1*, *FAN1*, *LG4*, *UVH1*, and *SOG1* (MvsF, MvsHF1, and MvsHF2) (Fig. 2D). Other non-differential expression profiles for DNA methylation, histone methylation, histone acetylation, and deacetylation genes showed that expression was stable (Fig. 2A–C). To conclude, 11 genes related to transcription regulation (*DDM1b*, *SUVH4b*, *SUVR4*, *JMJ13*, *JMJ26*, *HAC1c*, *HAF1*, *HDA8*, *HDA9*, *SRT1*, and *SRT2*) may represent potential regulators that specifically affect mRNA levels of several developmentally important key genes.

Expression of transposable elements Retand, Athila, *and* Copia *is up-regulated in hermaphrodites*

To derive genome-wide estimates of transcription at TE loci in a computationally efficient manner, we used SalmonTE (Jeong *et al.*, 2018). Based on a consensus TE sequence library of *S. latifolia* (Macas *et al.*, 2011), we estimated transcriptional signatures for 26 long terminal repeat (LTR) retroelements and five DNA transposons (Supplementary Dataset S3). From these clusters, *Copia1* Cl1 and *Copia2* Cl1, *Peabody* Cl13, and *LINE* Cl55 elements were differentially expressed such that expression levels were higher in males compared with females. Compared with males, androhermaphrodites (HF1 and HF2) differed mainly in *Copia* Cl15, *Ogre* Cl11, and the *Cassandra* retrotransposon, showing higher expression of *Copia* elements and lower expression for *Ogre* and *Cassandra* in HF1 (Supplementary Fig. S9; Supplementary Dataset S3). Compared with females, HF1 and HF2 differed additionally in *Gypsy* Cl13. These results show that some clusters of TEs, namely of *Copia* and *Gypsy* families, were deregulated in androhermaphrodites and this deregulation was inherited by two subsequent generations.

Detection of candidate genes in female floral development using GO enrichment, DEG, and clustering analysis

All differentially expressed transcripts and gene products were classified using GO enrichment analysis into groups involved in biological processes (BP), cellular components (CC), or molecular functions (MF) (Supplementary Figs S11, S12). Overall, 362 (4.49%) and 2296 (2.75%) of GO terms in BP, 83 (3.37%) and 525 (2.34%) in CC, and 372 (2.44%) and 479 (4.28%) of GO terms in MF were up- and down-regulated, respectively, in MvsHF1HF2 (differentially expressed between males and androhemraphrodites). In BP, the most enriched genes belong to cell division, cell cycle, polysaccharide catabolic, and isoprenoid/terpenoid metabolic processes. Among CC genes, the most enriched pathways are apoplast, microbody, and nucleus. MF genes were most affected in DNA-binding transcription factors and oxidoreductase activity (Supplementary Figs S10, S11). Among the genes with no classification or known function, 4 (9.9%) and 231 (3.18%) were up- and down-regulated, respectively, in MvsHF1HF2 (Supplementary Fig. S10, S11;(Supplementary Dataset S4). Among the up- and down-regulated transcripts in BP, we selected 213 genes that function in floral development (Supplementary Dataset S5). These include autosomal and sex-linked genes that were differentially expressed (up-regulated) in androhermaphrodites (Supplementary Dataset S5).

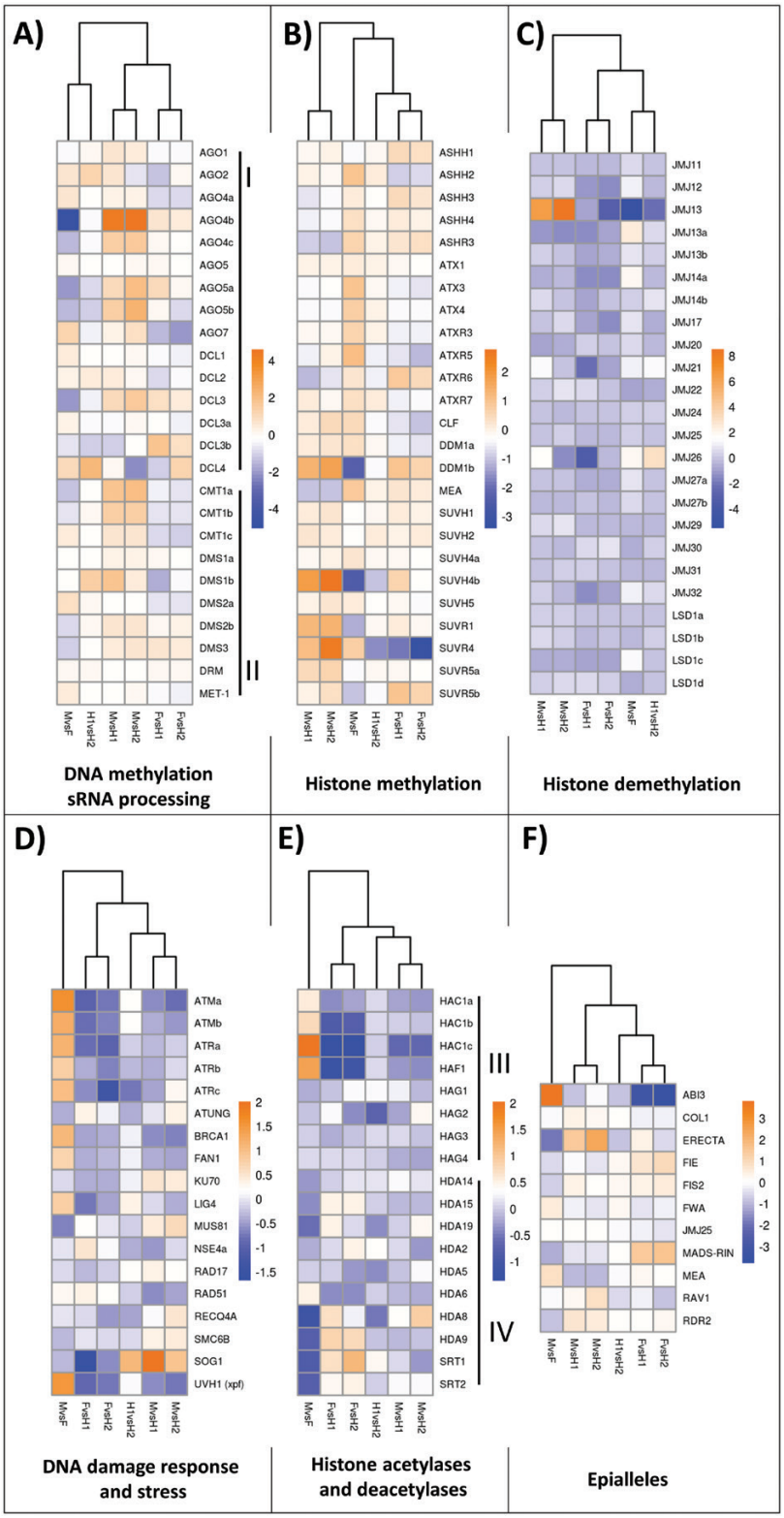

Fig. 2. Gene expression patterns related to androhermaphrodite development and transcriptome changes after the ZEB and SB treatment. (A) Genes involved in DNA methylation (I) and sRNA processing (II). (B) Genes associated with histone methylation. (C) Genes associated with histone lysine demethylation. (D) Genes involved in DNA damage response and stress. (E) Histone lysine acetylases (III) and deacetylases genes (IV). (F) Epialleles and genes regulated by DNA methylation. For corresponding gene IDs and literature sources, see Supplementary Table S3. Clusters show expression similarity between comparisons.

We looked for DEGs that were simultaneously down-regulated in MvsF, MvsHF1, and MvsHF2, and were sex-linked in all three comparisons in order to enrich the cluster of gynoecium-promoting candidates (female up-regulated genes in FHF1HF2, Fig. 3A). We additionally included in this cluster 10 sex-linked genes that were identified as androhermaphrodite specific compared with males and females (androhermaphrodite up-regulated genes in HF1HF2, Fig. 3A). These 45 sex-linked and 333 autosomal DEGs thus represent all possible candidates for gynoecium development (down-regulated in MvsF, MvsHF1, and MvsHF2) and were further designated as Group 1 (Supplementary Dataset S6). These DEGs were subsequently used in the second Venn diagram (Fig. 3B).

To identify all possible candidates which are related to gynoecium development in *S. latifolia*, we clustered all genes into five groups based on their expression levels using clustering analysis (Cl1–9): up-regulated in androhermaphrodites compared with males and females (Cl1–3), having similar levels of expression in androhermaphrodites and females (Cl4), strongly expressed in males and having low levels of expression in androhermaphrodites and females (Cl5, 6), down-regulated in androhermaphrodites compared with males and females (Cl7, 8), and having similar levels of expression among

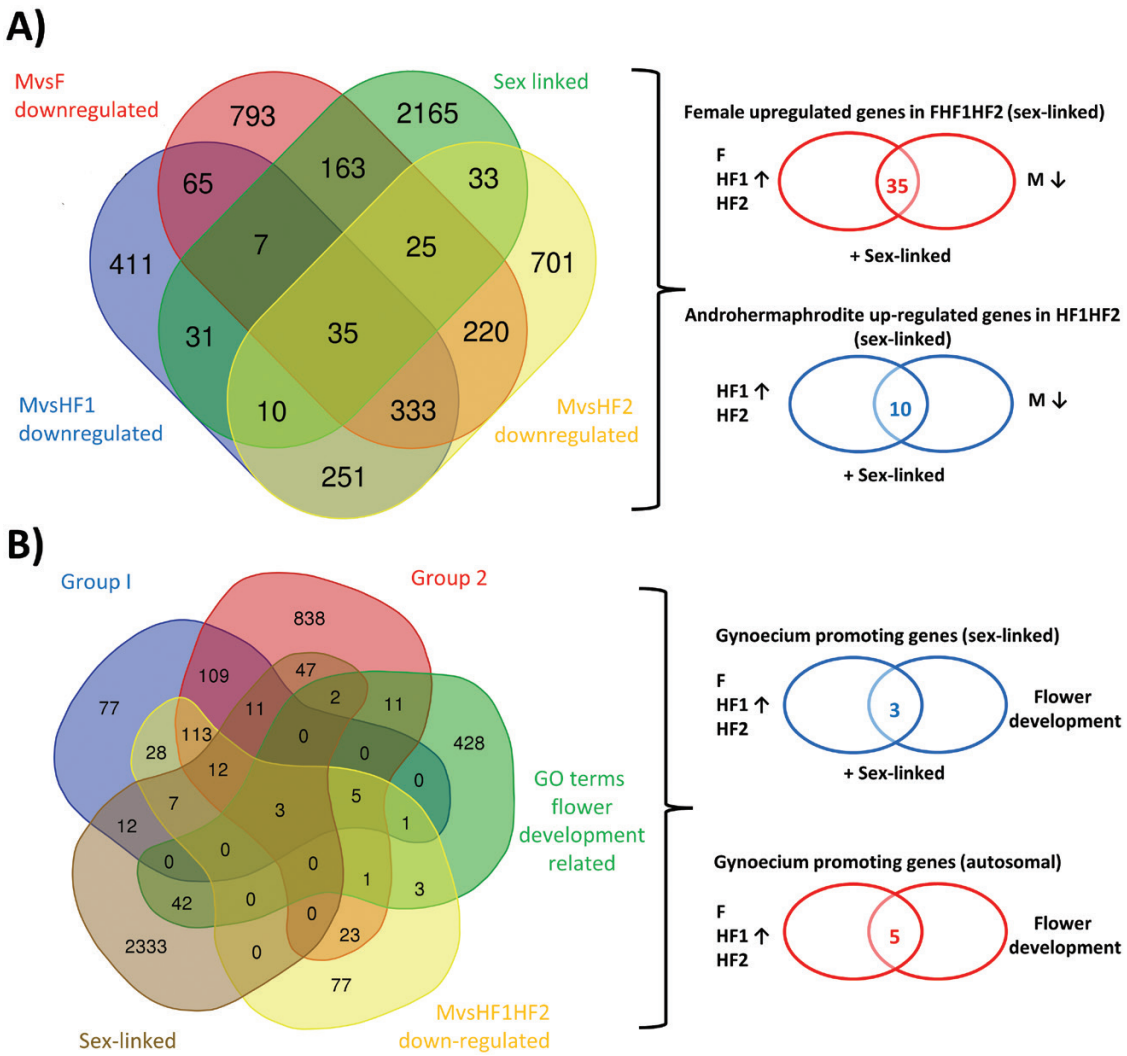

Fig. 3. Identification of candidate genes for gynoecium development using Venn diagrams. (A) Genes related to gynoecium development down-regulated in males compared with females and androhermaphrodites. The gene comparisons are as follows: MvsF down-regulated, MvsHF1 down-regulated, MvsHF2 down-regulated and sex-linked. From this comparison, all genes that were sex-linked and autosomal but simultaneously up-regulated in FHF1HF were designated as Group I (red and blue circles on the right) and used in the second Venn diagram. (B) Autosomal and sex-linked candidate genes involved in flower development and gynoecium promotion. The gene comparisons are as follows: Group I (MvsFHF1HF2 down-regulated), Group 2 (Cl4; Supplementary Fig. S12), GO terms associated with flower development (Supplementary Dataset S5), MvsHF1HF2 down-regulated (GO terms down-regulated MvsHF1HF2), and sex-linked candidates. Non-sex-linked genes enriched in GO terms associated with the flower development pathway were depicted as autosomal.

sexes (Cl9, Supplementary Fig. S12; (Supplementary Dataset S7). Cluster 4, designated in this study as Group 2, was further used in comparison of up-regulated genes between sexes and androhermaphrodites in the Venn diagram (Fig. 3B).

Identification of sex-specific candidates in gynoecium development

In order to reduce the gene numbers which were affected by the treatment and show a stable expression profile between generations, we compared all candidates that were identified based on GO (Supplementary Dataset 5), DEG (Supplementary Dataset 6), and clustering analysis (Supplementary Fig. S12; (Supplementary Dataset S7). This comparison newly identified three sex-linked and five autosomal potential candidates involved in gynoecium development based on Arabidopsis annotation (Fig. 3B; (Supplementary Dataset S8). The three candidates *GATA18 transcription factor*, known also as *HANABA TARANU* (*HAN or GATA18*); *AP2-like-responsive transcription factor AINTEGUMENTA* (*ANT*); and *Gibberellin 20 oxidase 1* (*GAOX1*; Supplementary Dataset S8) were up-regulated in androhermaphrodites compared with males, with higher levels of expression for *HAN* and *ANT* in females and *GAOX1* in androhermaphrodites (Fig. 4A). The five autosomal genes *SQUAMOSA promoter-binding protein-like transcription factor* (*SPL4*), *FRIGIDA-like protein 4a* (*FRL4a*), *Zinc finger protein WIP2* (*ZWIP2*), *Axial regulator YABBY1* (*YAB1*), and *homeobox protein ATH1* (*ATH1*) (Supplementary Dataset S8) were strongly expressed mainly in females and androhermaphrodites (Fig. 4A). Next, we were interested in the downstream regulatory gene pathways and the expression levels of the hypothetical binding partners described in Arabidopsis for all identified *Silene* candidates (Fig. 4B). Within the known regulatory pathway(s) were found specifically up-regulated genes with putative roles in gynoecium promotion and regulation of MADS-box genes, based on Arabidopsis annotation (Fig. 4B; Supplementary Dataset S8). Among these regulators, *SUP* (*SlSUP*) was found to be down-regulated in males and keeping intermediate expression in androhermaphrodites (Fig. 4B), suggesting a negative role in male organ development through regulation of B class MADS-box genes *PISTILATA* and *APETALA3a*. These two homologs were previously tested using *in situ* experiments, designated as *SLM2* and *SLM3* (Hardenack *et al.*, 1994). Similarly, *AS2* was found to be less expressed in males compared with androhermaphrodites and females. In males, the most different expression between upstream regulators in flower development was found for *NPR6* (*BOP1*) which is down-regulated in females (Fig. 4B). Additionally, androhermaphrodite transcriptome profiles showed higher expression of MADS-box genes class D, *PAN*, *REV1*, *AGL42*, and *JAGGED* compared with NT males, again genes identified as key regulators for the carpel development in the Arabidopsis model (Fig. 4B).

Discussion

The analysis of the androhermaphrodites in the two subsequent generations enabled us to show how multiple gene regulatory pathways are involved in flower development and in meristem maintenance of *S. latifolia*. In this study, we show that chemical genetics is a robust tool to analyse and examine novel regulatory pathways in floral development without genomic interference. We influenced the expression of female-specific genes, originally down-regulated in males, producing gene reactivation that led to gynoecium promotion in male flowers, turning males into androhermaphrodites. This flower trait was inherited only through the male germline (Supplementary Fig. S2), confirming previous results and holandric inheritance of the androhermaphrodite flower trait (Janoušek et al., 1996, 1998).

Androhermaphrodite flower development affects anther fertility and placenta organization

Androhermaphrodite development was examined using a combination of WFAD and ISEDS morphology-sensitive detectors, which allowed us to visualize detailed morphological changes at the cellular level (Fig. 1; Supplementary Fig. S4). Using these detectors, we obtained unique images of very large samples with high depth of field as well as specific details with high resolution and precision (Neděla *et al.*, 2015, 2016), compared with fixation-based electron micrographs of *S. latifolia* flowers (Uchida *et al.*, 2003; Koizumi *et al.*, 2007; Kazama *et al.*, 2016; Kawamoto *et al.*, 2019). Previous studies examining the infection of *Microbotryum lychnidis-dioicae* in male flowers using conventional SEM showed changes in infected females in earlier flower stages. This revealed the differences between males and females in the onset of teliospore formation (Uchida *et al.*, 2003). In addition, infection promoted stamen development in female flowers and elongation of filaments in asexual mutants, as in NT males. Yet, the gynoecium was suppressed within the same asexual flower (Kawamoto *et al.*, 2019). In this study, we observed slightly different changes in male and female development. NT male flowers contained a suppressed gynoecium and 10 (two whorls) fully developed stamens with viable pollen (Fig. 1B; Supplementary Fig. S5A, I). Androhermaphrodite flowers $HF_{III–IV}$ contained a gynoecium with a fully developed ovary and 1–3 stigmas, a suppressed stigma, and a significantly higher number ($P<0.001$) of aborted pollen grains (Fig. 1D, I–K; Supplementary Fig. S5B–F, I). Still, the androhermaphrodites produced 10 functional anthers in two whorls, and the gynoecium possessed fewer ovules. The ovule number could also be influenced by the age of the plant (Yuan and Kessler, 2019); therefore, we scored only the first 10 flowers after inflorescence initiation in each measurement (Supplementary Fig. S6). The lower androhermaphrodite fertility in comparison with the NT males and NT females also suggests that additional organ development may affect fitness

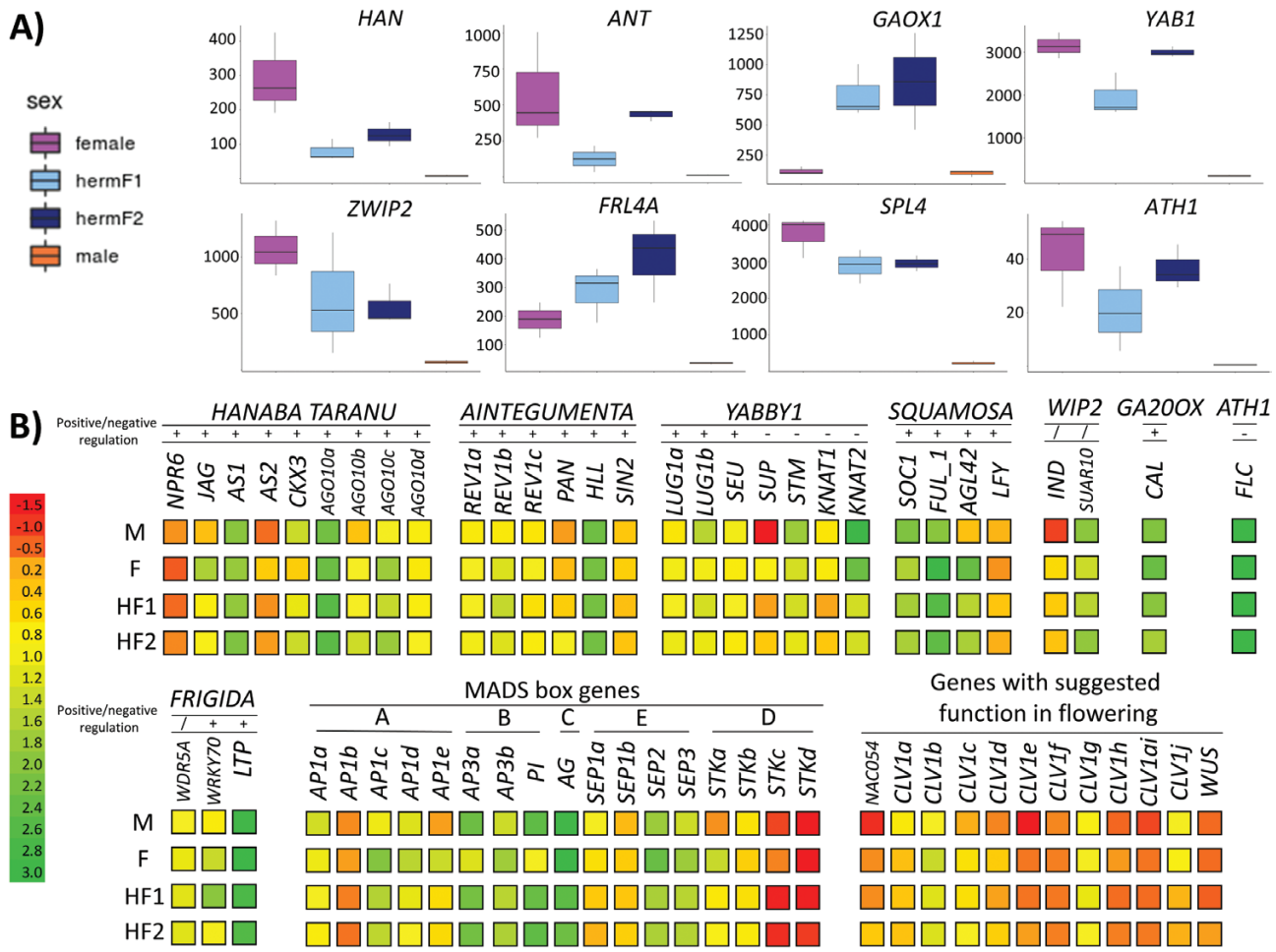

Fig. 4. The relative expression of candidate genes and their downstream known targets in Arabidopsis. (A) The expression of eight candidate genes involved gynoecium development (Fig. 3B, Gynoecium promoting genes). (B) The relative gene expression of selected genes which are known to be either positively (+) or negatively (–) regulated by the gynoecium promoting candidates, or they interact (/) with other transcription factors and proteins (the role or their interaction is inferred from the described regulatory pathways in Arabidopsis; Supplementary Dataset S8). MADS-box genes in ABC floral development were identified based on the available data in the Arabidopsis model (Supplementary Dataset S8). Genes with the suggested function were selected from previous studies in *Silene*, analyzed by other authors (Hardenack *et al.*, 1994; Deyhle *et al.*, 2007; Zluvova *et al.*, 2007; Koizumi *et al.*, 2010; Kazama *et al.*, 2012).

cost which can be higher for the bisexual flowers. These findings would be interesting to compare with the closely related gynodioecious species in further studies.

Androhermaphrodite flower trait-related expression changes

Rapid transcriptional changes in androhermaphrodite flowers inherited through the male germline in *S. latifolia* affected 103 sex-linked and 1706 non-sex-linked genes in HF1 and 153 sex-linked and 2468 non-sex-linked genes in HF2 (Supplementary Table S5). This is similar to the values based on the GO enrichment analysis, in which GO terms related to chemical treatment response reached from 2.44% to 4.49% of down-regulated and from 2.34% to 4.28% of up-regulated genes in androhermaphrodites (down-regulated in males; Supplementary Dataset S4). Thus, our results indicate that expression changes with stable ratio profiles may affect only a small percentage of regulatory genes in a heritable fashion and that only a small subset of genes are up- or down-regulated in response to chemical treatment, based on the GO enrichment analysis. In Arabidopsis, application of histone methylase and histone deacetylation inhibitors had non-redundant effects that affected only 3–4% of genes (from a total of 7800 monitored genes) (Chang and Pikaard, 2005), similar to this study. Further, the number of affected genes in this study is not different from the number of genes affected by smut fungus (4.7% of non-sex-linked and 7.2% of sex-linked genes up- or down-regulated) (Zemp *et al.*, 2015).

It is tempting to speculate that a small number of affected genes are inherited by subsequent generations and regulated by similar epigenetic mechanism (Janoušek *et al.*, 1996; Baubec *et*

al., 2014; Niederhuth and Schmitz, 2014). Although ZEB affects global DNA methylation in a dose-dependent and transient manner, independent of cytosine context (Baubec *et al.*, 2009; Griffin *et al.*, 2016), epigenetic inheritance from parents with divergent epigenomes permits long-lasting epiallelic interactions (Madlung *et al.*, 2002; Reinders *et al.*, 2009; Zhao *et al.*, 2011). The similar expression pattern between the first and the second generation of androhermaphrodites shows stable inheritance of the expression profiles for the studied genes. The fact that we identified only a small number of histone modification- and DNA methylation-related genes (i.e. *DDM1b*, *SUVH4b*, *SUVR4*, *JMJ13*, *JMJ26*, *HAC1c*, *HAF1*, *HDA8*, *HDA9*, *SRT1*, and *SRT2*; Fig. 2) with strong expression differences between males, females, and androhermaphrodites suggests that these genes may have a role in regulation of several pathways related to sex expression differences in *S. latifolia*. These genes may, among other functions, have a role in flower development as shown in other plant species (Vanyushin and Ashapkin, 2011; She and Baroux, 2014). Further, DNA damage- and stress-related homologous genes, which were previously shown to be expressed in Arabidopsis as responsive to chemical treatment (Liu *et al.*, 2015; Nowicka *et al.*, 2020), were expressed only in NT males compared with females and androhermaphrodites (i.e. *ATMa*, *ATMb*, *ATRa*, *ATRb*, *ATRc*, *BRCA1*, *FAN1*, *LG4*, *UVH1*, and *SOG1*) (Fig. 2D). It would be interesting to test in further studies whether the expression of these genes which is low in androhermaphrodites is needed to ensure the viability of pollen grains (Fig. 2D). The different expression of Arabidopsis homologs *ABI3* and *ERECTA* is not surprising, as both genes affect embryo development and inflorescence architecture, and must be present if the ovary is formed (Fig. 2C).

The difference in TE expression between males and females is in agreement with previous results showing specific proliferation of those repeats in separate sexes (Hobza *et al.*, 2015; Puterova *et al.*, 2018). However, the differences in expression of *Copia* and *Gypsy* elements is surprising because TEs are kept inactive in plants by transcriptional gene silencing (TGS), which provides a checkpoint for correct epigenetic inheritance during the transition from the vegetative to reproductive stage, as shown in Arabidopsis (Baubec *et al.*, 2014; Pecinka and Liu, 2014). Additionally, it was shown that ZEB induces transcriptional reactivation for TEs only in embryonic tissue (before flowering) (Baubec *et al.*, 2014). Thus, this result suggests not only that a subset of genes *de novo* up-regulated in *S. latifolia* androhermaphrodites is skewing the epigenetic inactivation but also that some clusters of *Copia* and *Gypsy* elements are deregulated with stable epigenetic inheritance, escaping the TGS regulatory pathway (Supplementary Fig. S9; Supplementary Dataset S3).

Candidate genes for gynoecium development include essential regulator transcription factors

Eight candidates identified in this study, namely *HAN*, *ANT*, *GAOX1*, *SPL4, FRL4a*, *ZWIP2*, *YAB1*, and *ATH1* (Fig. 3B), and their potential downstream regulated targets (based on Arabidopsis annotation) have the largest expression differences between males, females, HF1, and HF2 (Fig. 4A, B). Among the eight candidates, none was previously reported in *S. latifolia* (reviewed in Hobza *et al.*, 2018; Charlesworth, 2019) as sex linked or as putative candidates in female fower development. In Arabidopsis, all eight genes have a role in determination of flower size and morphology (Alvarez-Buylla *et al.*, 2010), and the strongest candidate *HAN* has an irreplaceable role in the meristem to organ transition, flower organization, and meristem boundary discrimination (Behringer and Schwechheimer, 2015; Ding *et al.*, 2015; Yu and Huang, 2016; Cucinotta *et al.*, 2020). Thus, we suggest that the *S. latifolia HAN* may directly determine meristem boundaries in developing flowers based on gene-specific up-regulation in androhermaphrodites compared with NT male flowers. This is supported by previous evidence for floral MADS-box genes in early developmental floral stages. The authors suggested that gynoecium-suppressing genes may act on the factors that determine the boundaries of the whorls (Hardenack *et al.*, 1994). If this is true, a *HAN* homolog is an ideal candidate. Nevertheless, it remains to be determined if *Silene HAN* promotes gynoecium development through regulation of its *Silene* homologs *YAB1*, *JAGGED*, and *CKX3* and its own autoregulation as showed in Arabidopsis (Ding *et al.*, 2015; Yu and Huang, 2016). *SUPERMAN-like* (*SlSUP*), previously reported as a negative regulator of male organ development in *S. latifolia* (Kazama *et al.*, 2009; Fujita *et al.*, 2019), was also specifically up-regulated in females, having intermediate expression in androhermaphrodites. Recently, Xu *et al.* (2018) suggested that in Arabidopsis SUP may regulate *APETALA3* and *PISTILATA* through regulation of the auxin level between whorl 3 and 4. Although, we do not have any such evidence regarding auxin homeostasis in *S. latifolia*, homologs of *PI* (SLM2) and *AP3* (SLM3) are down-regulated in females in our dataset, corroborating previous evidence of the negative role of the *SlSUP* allele in anther development (Fig. 4B). Interestingly, *YAB1* is up-regulated in females and to a lesser extent in hermaphrodites. This is correlated to a slight up-regulation of *SlSUP* in hermaphrodites which could explain the lower male fertility in HF1 and HF2. We suggest that *SlSUP* expression in *S. latifolia* is controlled by an unknown Y-linked regulator (Fig. 5A), and its low expression in androhermaphrodites is needed for proper carpel development together with intermediate expression of *HAN* and *ANT* (Fig. 5B, C). We hypothesize that sex determination takes place after the flower meristem is partioned into four concentric whorls of primordial cells, and that these key regulators, namely *SlSUP* and *HAN*, are among the first genes to be affected by the sex determination factor, which is yet to be identified (Hardenack *et al.*, 1994; Hobza *et al.*, 2018; Müller *et al.*, 2020). Despite correlated expression of newly identified genes in androhermaphrodites in this study, it should be stressed that some genes may have a role in only a few

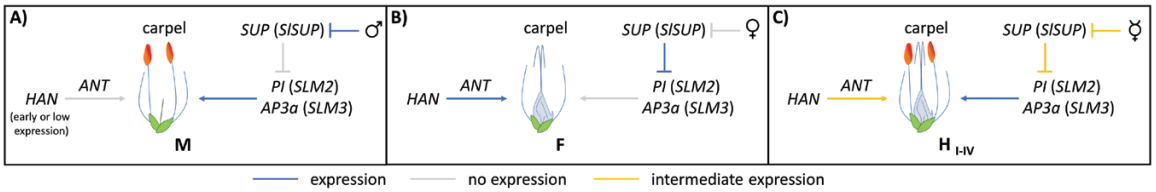

Fig. 5. The genetic model for carpel development in the dioecious plant *S. latifolia*. (A) The male develops stamens in the absence of *SlSUP* which is expressed in the central whorl based on *in situ* experiments in previous studies (Kazama *et al.*, 2009). The *SlSUP* gene is being suppressed by an unknown Y-linked mechanism in males. Simultaneously, *HAN* and *ANT* need to be down-regulated. (B) In females, *SlSUP* is up-regulated, affecting the expression of *PI* (*SLM2*) and *AP3a* (*SLM3*). *SlSUP* together with *HAN* and *ANT* are needed for proper carpel development. The stamen development is halted. (C) The male turns into an androhermaphrodite in the presence of DNA demethylation and histone deacetylation inhibitors, leading to intermediate *SlSUP*, *HAN*, and *ANT* expression. The androhermaphrodite flower consists of a fully developed carpel with a low number of ovules, and stamens which possess a higher number of non-viable pollen.

developmental stages. Further, the mapping efficiency to the reference transcriptome reached around 72–79%. Therefore, we would like to leave open the possibility that some other genes which were not mapped or might be expressed only during early flower development were not detected.

According to the classical model of ABC flowering development in *Arabidopsis thaliana*, and phenotype and expression analysis in this study, we suggest that androhermaphrodites (genetically males) possess a larger area in the central whorl (Fig. 1D), keeping the morphology of NT male flowers with a strongly enlarged gynoecium (carpel and two or three stigmas). This would be supported by the fact that the males contained 10 anthers and a suppressed gynoecium (two whorls), whereas females possessed only one central carpel with five stigmas and five suppressed anthers (two whorls) (Fig. 1B, C). Thus, androhermaphrodite flower of *S. latifolia* should resemble the ancestral state of flower organization as in the gynodioecious species *S. vulgaris* which possesses both a carpel with three stigmas and 10 anthers (Dulberger and Horovitz, 1984; Jürgens, 2006).

Furthermore, it remains unclear how epigenetic modifications regulate sex and flower morphology in *S. latifolia*. The morphological changes after application of chemical genetics show that sex determination in *S. latifolia* is influenced by an epigenetic-related pathway, as previously reported in *Diospyros kaki* (Akagi *et al.*, 2016). To understand the role of epigenetic control during male and female flower development, it will be necessary to obtain the complete methylation profiles from bisulfite-treated DNA. Further, a comparison of male and female transcriptome profiles obtained from infected individuals by smut fungus and individuals treated by chemical compounds would yield new potential candidates in male organ development. Such candidates can be further tested by the use of genetic transformation and targeted mutagenesis protocols that are now available for *S. latifolia* (Hudzieczek *et al.*, 2019). Such approaches will also simplify further studies of each of the candidate genes in this study and their functions in relation to sex determination, namely homologs of *HAN*, *ANT*, and *SlSUP*. Our study shows that the expression of these three candidates is essential in gynoecium development and further supports the role of *SlSUP* in sex determination in *S. latifolia*.

Supplementary data

The following supplementary data are available at *JXB* online.

Fig. S1. The schematic representation of inhibitor screening and workflow.

Fig. S2. The schematic pedigree of androhermaphrodite inheritance in the progeny.

Fig. S3. The effect of zebularine and sodium butyrate on seedlings of *S. latifolia* U15.

Fig. S4. FE-ESEM of a WT female and a female of the androhermaphrodite progeny.

Fig. S5. Viability staining and FE-ESEM of WT and androhermaphrodite pollen.

Fig. S6. Comparison of different carpel developmental stages observed in the androhermaphrodite progeny.

Fig. S7. Data validation of RNA-seq data obtained from studied transcriptomes.

Fig. S8. Volcano plots.

Fig. S9. The repeat expression profiles in androhermaphrodites.

Fig. S10. Gene Ontology enrichment A.

Fig. S11. Gene Ontology enrichment B.

Fig. S12. Clustering analysis.

Table S1. Reference transcriptome annotation by the Trinotate pipeline.

Table S2. Numbers of sex-linked genes/transcripts identified in the reference transcriptome by blast searches with sex-linked gene databases from several publications.

Table S3. Sequencing read trimming and pseudoaligning statistics.

Table S4. BUSCO output of the *S. latifolia* U14 reference transcriptome.

Table S5. Number of differentially expressed genes between the sexes.

Dataset S1. ID and total number of DEGs.

Dataset S2. DNA- and histone-modifying genes.

Dataset S3. Repeat expression.

Dataset S4. GO analysis of up- and down-regulated genes.

Dataset S5. GO analysis categories and GO flower development genes.

Dataset S6. Hermaphrodite and female up-regulated sex-linked and autosomal genes.

Dataset S7. Clustering analysis.

Dataset S8. Flower-related genes.

Appendix S1. List of software and tools used, ZEB and SB comparison.

Acknowledgements

We would like to thank Peridot Scientific Communications Plant Editors Team for the English language correction. We thank the EMBL Genomics Core Facility (EMBL, Heidelberg) for transcriptome sequencing, and Dr Aline Muyle for the *S. litifolia* sex-linked genes identified by SEX-DETector. Computational resources were supplied by the project 'e-Infrastruktura CZ' (e-INFRA LM2018140) provided within the program Projects of Large Research, Development and Innovations Infrastructures.

Author contributions

VBac, RC, and RH: conceptualization of the project and research plans; VBac, LS, TJ, and VH, RC, VBen, ET, and VN: performing the experiments; RC and VBen: data analysis; VBac, RC, and RH: research design and data interpretation; VBac: writing with contributions of all the authors.

Conflict of interest

The authors declare no conflict of interest.

Funding

This project was supported by the Czech Science Foundation (numbers 19-02476Y and 22-25799S) and by the Czech Academy of Sciences (RVO:68081731).

Data availability

All data supporting the findings of this study are available within the paper and within its supplementary data published online. The transcriptome sequencing data are deposited in the European Nucleotide Archive (https://www.ebi.ac.uk/ena/browser/home) under accession no. PRJEB36078 and in the Dryad Digital Repository https://doi.org/10.5061/dryad.t1g1jwt2v; Bačovský *et al.* (2022).

References

Abbott JK, Nordén AK, Hansson B. 2017. Sex chromosome evolution: historical insights and future perspectives. Proceedings of the Royal Society B: Biological Sciences **284**, 20162806

Akagi T, Henry IM, Kawai T, Comai L, Tao R. 2016. Epigenetic regulation of the sex determination gene MeGI in polyploid persimmon. The Plant Cell **28**, 2905–2915.

Akagi T, Henry IM, Tao R, Comai L. 2014. A Y-chromosome-encoded small RNA acts as a sex determinant in persimmons. Science **346**, 646– 650.

Akagi T, Pilkington SM, Varkonyi-Gasic E, *et al.* 2019. Two Y-chromosome-encoded genes determine sex in kiwifruit. Nature Plants **5**, 801–809.

Alvarez-Buylla ER, Benítez M, Corvera-Poiré A, *et al.* 2010. Flower development. The Arabidopsis Book **8**, e0127.

Bačovský V, Houben A, Kumke K, Hobza R. 2019. The distribution of epigenetic histone marks differs between the X and Y chromosomes in *Silene latifolia*. Planta **250**, 487–494.

Bačovský V, Čegan R, Tihlaříková E, Neděla V, Hudzieczek V, Smrža L, Janíček T, Beneš V, Hobza R. 2022. Data from: Chemical genetics in *Silene latifolia* elucidate regulatory pathways involved in gynoecium development. Dryad Digital Repository doi: 10.5061/dryad.t1g1jwt2v.

Bartels A, Han Q, Nair P, *et al.* 2018. Dynamic DNA methylation in plant growth and development. International Journal of Molecular Science **19**, 2144

Baubec T, Dinh HQ, Pecinka A, Rakic B, Rozhon W, Wohlrab B, von Haeseler A, Mittelsten Scheid O. 2010. Cooperation of multiple chromatin modifications can generate unanticipated stability of epigenetic states in Arabidopsis. The Plant Cell **22**, 34–47.

Baubec T, Finke A, Mittelsten Scheid O, Pecinka A. 2014. Meristem-specific expression of epigenetic regulators safeguards transposon silencing in Arabidopsis. EMBO Reports **15**, 446–452.

Baubec T, Pecinka A, Rozhon W, Mittelsten Scheid O. 2009. Effective, homogeneous and transient interference with cytosine methylation in plant genomic DNA by zebularine. The Plant Journal **57**, 542–554.

Behringer C, Schwechheimer C. 2015. B-GATA transcription factors—insights into their structure, regulation, and role in plant development. Frontiers in Plant Science **6**, 90.

Bergero R, Charlesworth D. 2011. Preservation of the Y transcriptome in a 10-million-year-old plant sex chromosome system. Current Biology **21**, 1470–1474.

Bolger AM, Lohse M, Usadel B. 2014. Trimmomatic: a flexible trimmer for Illumina sequence data. Bioinformatics **30**, 2114–2120.

Bräutigam K, Soolanayakanahally R, Champigny M, Mansfield S, Douglas C, Campbell MM, Cronk Q. 2017. Sexual epigenetics: gender-specific methylation of a gene in the sex determining region of *Populus balsamifera*. Scientific Reports **7**, 45388.

Bray NL, Pimentel H, Melsted P, Pachter L. 2016. Near-optimal probabilistic RNA-seq quantification. Nature Biotechnology **34**, 525–527.

Bryant DM, Johnson K, DiTommaso T, *et al.* 2017. A tissue-mapped axolotl de novo transcriptome enables identification of limb regeneration factors. Cell Reports **18**, 762–776.

Chang S, Pikaard CS. 2005. Transcript profiling in Arabidopsis reveals complex responses to global inhibition of DNA methylation and histone deacetylation. Journal of Biological Chemistry **280**, 796–804.

Charlesworth D. 2016. Plant sex chromosomes. Annual Review of Plant Biology **67**, 397–420.

Charlesworth D. 2019. Young sex chromosomes in plants and animals. New Phytologist **224**, 1095–1107.

Chibalina MV, Filatov DA. 2011. Plant Y chromosome degeneration is retarded by haploid purifying selection. Current Biology **21**, 1475–1479.

Cronk Q, Müller NA. 2020. Default sex and single gene sex determination in dioecious plants. Frontiers in Plant Science **11**, 1162.

Cruz DR, Becker C. 2020. A critical guide for studies on epigenetic inheritance in plants. Methods in Molecular Biology **2093**, 261–270.

Cucinotta M, Di Marzo M, Guazzotti A, de Folter S, Kater MM, Colombo L. 2020. Gynoecium size and ovule number are interconnected traits that impact seed yield. Journal of Experimental Botany **71**, 2479–2489.

Deyhle F, Sarkar AK, Tucker EJ, Laux T. 2007. WUSCHEL regulates cell differentiation during anther development. Developmental Biology **302**, 154–159.

Ding L, Yan S, Jiang L, Zhao W, Ning K, Zhao J, Liu X, Zhang J, Wang Q, Zhang X. 2015. HANABA TARANU (HAN) bridges meristem and organ primordia boundaries through PINHEAD, JAGGED, BLADE-ON-PETIOLE2 and CYTOKININ OXIDASE 3 during flower development in Arabidopsis. PLoS Genetics **11**, e1005479.

Dulberger R, Horovitz A. 1984. Gender polymorphism in flowers of *Silene vulgaris* (Moench) Garcke (Caryophyllaceae). Botanical Journal of the Linnean Society **89**, 101–117

Fujita N, Kazama Y, Yamagishi N, Watanabe K, Ando S, Tsuji H, Kawano S, Yoshikawa N, Komatsu K. 2019. Development of the VIGS system in the dioecious plant *Silene latifolia*. International Journal of Molecular Science **20**, 1031.

Glazinska P, Wojciechowski W, Kulasek M, Glinkowski W, Marciniak K, Klajn N, Kesy J, Kopcewicz J. 2017. De novo transcriptome profiling of flowers, flower pedicels and pods of *Lupinus luteus* (yellow lupine) reveals complex expression changes during organ abscission. Frontiers in Plant Science **8**, 641.

Griffin PT, Niederhuth CE, Schmitz RJ. 2016. A comparative analysis of 5-azacytidine- and zebularine-induced DNA demethylation. G3 **6**, 2773–2780.

Hardenack S, Ye D, Saedler H, Grant S. 1994. Comparison of MADS box gene expression in developing male and female flowers of the dioecious plant white campion. The Plant Cell **6**, 1775–1787.

Harkess A, Zhou J, Xu C, *et al.* 2017. The asparagus genome sheds light on the origin and evolution of a young Y chromosome. Nature Communications **8**, 1279.

Hobza R, Hudzieczek V, Kubat Z, Cegan R, Vyskot B, Kejnovsky E, Janousek B. 2018. Sex and the flower—developmental aspects of sex chromosome evolution. Annals of Botany **122**, 1085–1101

Hobza R, Kubat Z, Cegan R, Jesionek W, Vyskot B, Kejnovsky E. 2015. Impact of repetitive DNA on sex chromosome evolution in plants. Chromosome Research **23**, 561–570.

Howlader J, Robin AHK, Natarajan S, Biswas MK, Sumi KR, Song CY, Park J, Nou I. 2020. Transcriptome analysis by RNA-Seq reveals genes related to plant height in two sets of parent–hybrid combinations in easter lily (*Lilium longiflorum*). Scientific Reports **10**, 9082.

Hu J, Liu Y, Tang X, Rao H, Ren C, Chen J, Wu Q, Jiang Y, Geng F, Pei J. 2020. Transcriptome profiling of the flowering transition in saffron (*Crocus sativus* L.). Scientific Reports **10**, 9680.

Hudzieczek V, Cegan R, Cermak T, Bacovska N, Machalkova Z, Dolezal K, Plihalova L, Voytas D, Hobza R, Vyskot B. 2019. *Agrobacterium rhizogenes*-mediated transformation of a dioecious plant model *Silene latifolia*. New Biotechnology **48**, 20–28.

Hurst LD. 1996. Why are there only two sexes? Proceedings of the Royal Society B: Biological Sciences **263**, 415–422

Janoušek B, Grant SR, Vyskot B. 1998. Non-transmissibility of the Y chromosome through the female line in androhermaphrodite plants of *Melandrium album*. Heredity **80**, 576–583

Janousek B, Siroký J, Vyskot B. 1996. Epigenetic control of sexual phenotype in a dioecious plant, *Melandrium album*. Molecular & General Genetics **250**, 483–490.

Jeong HH, Yalamanchili HK, Guo C, Shulman JM, Liu Z. 2018. An ultra-fast and scalable quantification pipeline for transposable elements from next generation sequencing data. Pacific Symposium on Biocomputing **23**, 168–179.

Jürgens A. 2006. Comparative floral morphometrics in day-flowering, night-flowering and self-pollinated Caryophylloideae (*Agrostemma*, *Dianthus*, *Saponaria*, *Silene*, and *Vaccaria*). Plant Systematics and Evolution **257**, 233–250

Kang WH, Sim YM, Koo N, Nam JY, Lee J, Kim N, Jang H, Kim YM, Yeom SI. 2020. Transcriptome profiling of abiotic responses to heat, cold, salt, and osmotic stress of *Capsicum annuum* L. Scientific Data **7**, 17.

Kawamoto H, Yamanaka K, Koizumi A, Ishii K, Kazama Y, Abe T, Kawano S. 2019. An asexual flower of *Silene latifolia* and *Microbotryum lychnidis-dioicae* promotes sex-organ development. PLoS One **14**, e0217329.

Kazama Y, Fujiwara MT, Koizumi A, Nishihara K, Nishiyama R, Kifune E, Abe T, Kawano S. 2009. A SUPERMAN-like gene is exclusively expressed in female flowers of the dioecious plant *Silene latifolia*. Plant & Cell Physiology **50**, 1127–1141.

Kazama Y, Ishii K, Aonuma W, *et al.* 2016. A new physical mapping approach refines the sex-determining gene positions on the *Silene latifolia* Y-chromosome. Scientific Reports **6**, 18917.

Kazama Y, Koizumi A, Uchida W, Ageez A, Kawano S. 2005. Expression of the floral B-function gene SLM2 in female flowers of *Silene latifolia* infected with the smut fungus *Microbotryum violaceum*. Plant & Cell Physiology **46**, 806–811.

Kazama Y, Nishihara K, Bergero R, Fujiwara MT, Abe T, Charlesworth D, Kawano S. 2012. SlWUS1 an X-linked gene having no homologous Y-linked copy in *Silene latifolia*. **2**, 1269–1278

Koizumi A, Amanai Y, Ishii K, Nishihara K, Kazama Y, Uchida W, Kawano S. 2007. Floral development of an asexual and female-like mutant carrying two deletions in gynoecium-suppressing and stamen-promoting functional regions on the Y chromosome of the dioecious plant *Silene latifolia*. Plant & Cell Physiology **48**, 1450–1461.

Koizumi A, Yamanaka K, Nishihara K, Kazama Y, Abe T, Kawano S. 2010. Two separate pathways including SlCLV1, SlSTM and SlCUC that control carpel development in a bisexual mutant of *Silene latifolia*. Plant & Cell Physiology **51**, 282–293.

Kumar S, Trivedi PK. 2016. Transcriptome modulation in rice under abiotic stress. In: Azooz MM, Ahmad P, eds. Plant–environment interactions: responses and approaches to mitigate stress. Chichester, UK: Wiley, 70–83.

Lechner T, Lusser A, Brosch G, Eberharter A, Goralik-Schramel M, Loidl P. 1996. A comparative study of histone deacetylases of plant, fungal and vertebrate cells. Biochimica et Biophysica Acta **1296**, 181–188.

Li X, Wei Y, Nettleton D, Brummer EC. 2009. Comparative gene expression profiles between heterotic and non-heterotic hybrids of tetraploid *Medicago sativa*. BMC Plant Biology **9**, 107.

Liu CH, Finke A, Díaz M, Rozhon W, Poppenberger B, Baubec T, Pecinka A. 2015. Repair of DNA damage induced by the cytidine analog zebularine requires ATR and ATM in Arabidopsis. The Plant Cell **27**, 1788–1800.

Love MI, Huber W, Anders S. 2014. Moderated estimation of fold change and dispersion for RNA-seq data with DESeq2. Genome Biology **15**, 550.

Macas J, Kejnovský E, Neumann P, Novák P, Koblížková A, Vyskot B. 2011. Next generation sequencing-based analysis of repetitive DNA in the model dioceous plant *Silene latifolia*. PLoS One **6**, e27335.

Madlung A, Masuelli RW, Watson B, Reynolds SH, Davison J, Comai L. 2002. Remodeling of DNA methylation and phenotypic and transcriptional changes in synthetic Arabidopsis allotetraploids. Plant Physiology **129**, 733–746.

Mortazavi A, Williams BA, McCue K, Schaeffer L, Wold B. 2008. Mapping and quantifying mammalian transcriptomes by RNA-Seq. Nature Methods **5**, 621–628.

Müller NA, Kersten B, Leite Montalvão AP, *et al.* 2020. A single gene underlies the dynamic evolution of poplar sex determination. Nature Plants **6**, 630–637.

Muyle A, Zemp N, Deschamps C, Mousset S, Widmer A, Marais GA. 2012. Rapid de novo evolution of X chromosome dosage compensation in *Silene latifolia*, a plant with young sex chromosomes. PLoS Biology **10**, e1001308.

Neděla V, Hřib J, Havel L, Hudec J, Runštuk J. 2016. Imaging of Norway spruce early somatic embryos with the ESEM, Cryo-SEM and laser scanning microscope. Micron **84**, 67–71.

Neděla V, Tihlaříková E, Hřib J. 2015. The low-temperature method for study of coniferous tissues in the environmental scanning electron microscope. Microscopy Research and Technique **78**, 13–21.

Neděla V, Tihlaříková E, Maxa J, Imrichová K, Bučko M, Gemeiner P. 2020. Simulation-based optimisation of thermodynamic conditions in the ESEM for dynamical in-situ study of spherical polyelectrolyte complex particles in their native state. Ultramicroscopy **211**, 112954.

Neděla V, Tihlaříková E, Runštuk J, Hudec J. 2018. High-efficiency detector of secondary and backscattered electrons for low-dose imaging in the ESEM. Ultramicroscopy **184**, 1–11

Niederhuth CE, Schmitz RJ. 2014. Covering your bases: inheritance of DNA methylation in plant genomes. Molecular Plant **7**, 472–480.

Nowicka A, Tokarz B, Zwyrtková J, *et al.* 2020. Comparative analysis of epigenetic inhibitors reveals different degrees of interference with transcriptional gene silencing and induction of DNA damage. The Plant Journal **102**, 68–84.

Papadopulos AS, Chester M, Ridout K, Filatov DA. 2015. Rapid Y degeneration and dosage compensation in plant sex chromosomes. Proceedings of the National Academy of Sciences, USA **112**, 13021–13026.

Pecinka A, Liu CH. 2014. Drugs for plant chromosome and chromatin research. Cytogenetic and Genome Research **143**, 51–59.

Peterson R, Slovin JP, Chen C. 2010. A simplified method for differential staining of aborted and non-aborted pollen grains. International Journal of Plant Biology **1**, 13

Puterova J, Kubat Z, Kejnovsky E, Jesionek W, Cizkova J, Vyskot B, Hobza R. 2018. The slowdown of Y chromosome expansion in dioecious *Silene latifolia* due to DNA loss and male-specific silencing of retrotransposons. BMC Genomics **19**, 153.

Quan S, Niu J, Zhou L, Xu H, Ma L, Qin Y. 2019. Stages identifying and transcriptome profiling of the floral transition in *Juglans regia*. Scientific Reports **9**, 7092.

Reinders J, Wulff BB, Mirouze M, Marí-Ordóñez A, Dapp M, Rozhon W, Bucher E, Theiler G, Paszkowski J. 2009. Compromised stability of DNA methylation and transposon immobilization in mosaic Arabidopsis epigenomes. Genes & Development **23**, 939–950.

Renner SS. 2014. The relative and absolute frequencies of angiosperm sexual systems: dioecy, monoecy, gynodioecy, and an updated online database. American Journal of Botany **101**, 1588–1596.

Renner SS, Müller NA. 2021. Plant sex chromosomes defy evolutionary models of expanding recombination suppression and genetic degeneration. Nature Plants **7**, 392–402.

Rodríguez Lorenzo JL, Hobza R, Vyskot B. 2018. DNA methylation and genetic degeneration of the Y chromosome in the dioecious plant *Silene latifolia*. BMC Genomics **19**, 540.

Rodríguez Lorenzo JL, Hubinský M, Vyskot B, Hobza R. 2020. Histone post-translational modifications in *Silene latifolia* X and Y chromosomes suggest a mammal-like dosage compensation system. Plant Science **299**, 110528.

She W, Baroux C. 2014. Chromatin dynamics during plant sexual reproduction. Frontiers in Plant Science **5**, 354.

Shendure J, Balasubramanian S, Church GM, Gilbert W, Rogers J, Schloss JA, Waterston RH. 2017. DNA sequencing at 40: past, present and future. Nature **550**, 345–353.

Shulse CN, Cole BJ, Ciobanu D, *et al.* 2019. High-throughput single-cell transcriptome profiling of plant cell types. Cell Reports **27**, 2241–2247.

Simão FA, Waterhouse RM, Ioannidis P, Kriventseva EV, Zdobnov EM. 2015. BUSCO: assessing genome assembly and annotation completeness with single-copy orthologs. Bioinformatics **31**, 3210–3212.

Tanurdzic M, Banks JA. 2004. Sex-determining mechanisms in land plants. The Plant Cell 16 Suppl, S61–S71.

Uchida W, Matsunaga S, Sugiyama R, Kazama Y, Kawano S. 2003. Morphological development of anthers induced by the dimorphic smut fungus *Microbotryum violaceum* in female flowers of the dioecious plant *Silene latifolia*. Planta **218**, 240–248.

Vanyushin BF, Ashapkin VV. 2011. DNA methylation in higher plants: past, present and future. Biochimica et Biophysica Acta **1809**, 360–368.

Wang Z, Gerstein M, Snyder M. 2009. RNA-Seq: a revolutionary tool for transcriptomics. Nature Reviews. Genetics **10**, 57–63.

Westergaard M. 1946. Aberrant Y chromosomes and sex expression in *Melandrium album*. Hereditas **32**, 419–443.

Westergaard M. 1958. The mechanism of sex determination in dioecious flowering plants. Advances in Genetics **9**, 217–281.

Xu Y, Prunet N, Gan E-S, *et al*. 2018. SUPERMAN regulates floral whorl boundaries through control of auxin biosynthesis. The EMBO Journal **37**, e97499

Ye D, Installé P, Ciupercescu D, Veuskens J, Wu Y, Salesses G, Jacobs M, Negrutiu I. 1990. Sex determination in the dioecious *Melandrium*. Sexual Plant Reproduction **3**, 179–186

Young MD, Wakefield MJ, Smyth GK, Oshlack A. 2010. Gene ontology analysis for RNA-seq: accounting for selection bias. Genome Biology **11**, R14.

Yu H, Huang T. 2016. Molecular mechanisms of floral boundary formation in Arabidopsis. International Journal of Molecular Sciences **17**, 317.

Yuan J, Kessler SA. 2019. A genome-wide association study reveals a novel regulator of ovule number and fertility in *Arabidopsis thaliana*. PLoS Genetics **15**, e1007934.

Zemp N, Tavares R, Muyle A, Charlesworth D, Marais GA, Widmer A. 2016. Evolution of sex-biased gene expression in a dioecious plant. Nature Plants **2**, 16168.

Zemp N, Tavares R, Widmer A. 2015. Fungal infection induces sex-specific transcriptional changes and alters sexual dimorphism in the dioecious plant *Silene latifolia*. PLoS Genetics **11**, e1005536.

Zhang H, Lang Z, Zhu JK. 2018. Dynamics and function of DNA methylation in plants. Nature Reviews. Molecular Cell Biology **19**, 489–506.

Zhang H, Wang B, Duan C-G, Zhu J-K. 2013. Chemical probes in plant epigenetics studies. Plant Signal & Behavior **8**, 37–41.

Zhao N, Zhu B, Li M, Wang L, Xu L, Zhang H, Zheng S, Qi B, Han F, Liu B. 2011. Extensive and heritable epigenetic remodeling and genetic stability accompany allohexaploidization of wheat. Genetics **188**, 499–510.

Zluvova J, Georgiev S, Janousek B, Charlesworth D, Vyskot B, Negrutiu I. 2007. Early events in the evolution of the *Silene latifolia* Y chromosome: male specialization and recombination arrest. Genetics **177**, 375–386.

Zluvova J, Zak J, Janousek B, Vyskot B. 2010. Dioecious *Silene latifolia* plants show sexual dimorphism in the vegetative stage. BMC Plant Biology **10**, 208.